ELSEVIER

Nuclear Instruments and Methods in Physics Research B 193 (2002) 530–537

NIM B
Beam Interactions with Materials & Atoms

www.elsevier.com/locate/nimb

Comparative study of surface-lattice-site resolved neutralization of slow multicharged ions during large-angle quasi-binary collisions with Au(1 1 0): Simulation and experiment

F.W. Meyer *, V.A. Morozov

Physics Division, Oak Ridge National Laboratory, Oak Ridge, TN 37831-6372, USA

Abstract

In this article we extend our earlier studies of the azimuthal dependences of low energy projectiles scattered in large angle quasi-binary collisions (BCs) from Au(1 1 0). Measurements are presented for 20 keV Ar^{9+} at normal incidence, which are compared with our earlier measurements for this ion at 5 keV and 10° incidence angle. A deconvolution procedure based on MARLOWE simulation results carried out at both energies provides information about the energy dependence of projectile neutralization during interactions just with the atoms along the top ridge of the reconstructed Au(1 1 0) surface corrugation, in comparison to, e.g. interactions with atoms lying on the sidewalls. To test the sensitivity of the agreement between the MARLOWE results and the experimental measurements, we show simulation results obtained for a non-reconstructed Au(1 1 0) surface with 20 keV Ar projectiles, and for different scattering potentials that are intended to simulate the effects on scattering trajectory of a projectile inner shell vacancy surviving the BC. In addition, simulation results are shown for a number of different total scattering angles, to illustrate their utility in finding optimum values for this parameter prior to the actual measurements. © 2002 Elsevier Science B.V. All rights reserved.

PACS: 79.20.Rf; 79.20.Ap; 34.50.Dy; 61.18.Bn

1. Introduction

The large angle scattering technique has been used in a number of recent studies [1–5] of multicharged projectile neutralization during interactions with metal and insulator surfaces. By the use of energy and charge analysis of the backscattered projectiles, this method provides, e.g. insights into energy loss mechanisms accompanying projectile neutralization [2], and permits, in contrast to studies of grazing deflection events which result by cumulative scattering involving a large number of lattice sites [6], the resolution of interactions occurring with just one or two atoms located on the target surface.

In this article we have extended our previous studies [3,4] on multicharged projectile neutralization during binary and quasi-binary collisions (BCs) with atoms located on a Au(1 1 0) surface. First, we have measured the target azimuth dependence of scattered charge fractions for 20 keV

* Corresponding author. Tel.: +1-1-865-574-4705; fax: +1-1-865-574-1118.
E-mail address: meyerfw@ornl.gov (F.W. Meyer).

0168-583X/02/$ - see front matter © 2002 Elsevier Science B.V. All rights reserved.
PII: S0168-583X(02)00844-3

Ar^{9+} ions normally incident on Au(1 1 0), for comparison with similar measurements of 5 keV Ar^{9+} projectiles incident on Au(1 1 0) at 10°. In order to make an analysis of the contributions of the various Au(1 1 0) surface scattering sites and collision types similar to that already performed at 5 keV, we also carried out MARLOWE [7] trajectory simulations at the higher projectile energy and normal incidence angle. We report as well the results of some auxiliary MARLOWE studies in which we explored the sensitivity of the trajectory simulations to changes in the scattering potential intended to mimic the effects of incomplete neutralization, and to the surface topography itself, by comparing scattering from both reconstructed and unreconstructed Au(1 1 0) surfaces.

As has been noted previously, at the few to tens of keV impact energies studied in the present article, contributions to the overall projectile neutralization by "hollow atom" formation at large distances followed by Auger relaxation prior to surface-impact [8] are considered to be negligible, and multicharged ion (MCI) neutralization proceeds instead by the complex multi-electron processes occurring closer to the surface in the vicinity of the trajectory turning point. The goal of the present contribution is to demonstrate the potential of the large angle backscattering technique for such MCI-surface charge exchange studies at higher energies, and to explore what additional information the measured azimuth dependences might contain, either regarding the neutralization process or the surface topography itself.

2. Experiment

The measurements were carried out at the ORNL Multicharged Ion Research Facility with an apparatus that implements an ultra-high vacuum (10^{-10} mbar) floating scattering chamber and time-of-flight (TOF) analyzer with floatable drift tube [9–11], permitting simultaneous measurements of energy distributions and charge fractions of projectiles scattered from the single crystal target into 120°. The target was attached to a sample mount with two rotational degrees of freedom and was prepared by cycles of sputter cleaning under grazing incidence with 2 keV Ar^{+} ions and successive annealing cycles at about 450 °C. The chopped primary beams of argon MCI were decelerated from $(10 \times q)$ keV to their final energy before impinging on the Au(1 1 0) surface.

Fig. 1 shows a typical scattered projectile TOF spectrum for 20 keV Ar^{9+} ions incident normally on Au(1 1 0). The figure illustrates the degree of charge state separation obtainable at this energy using the maximum drift tube voltage of −4 kV achievable with the present set-up. As can be seen

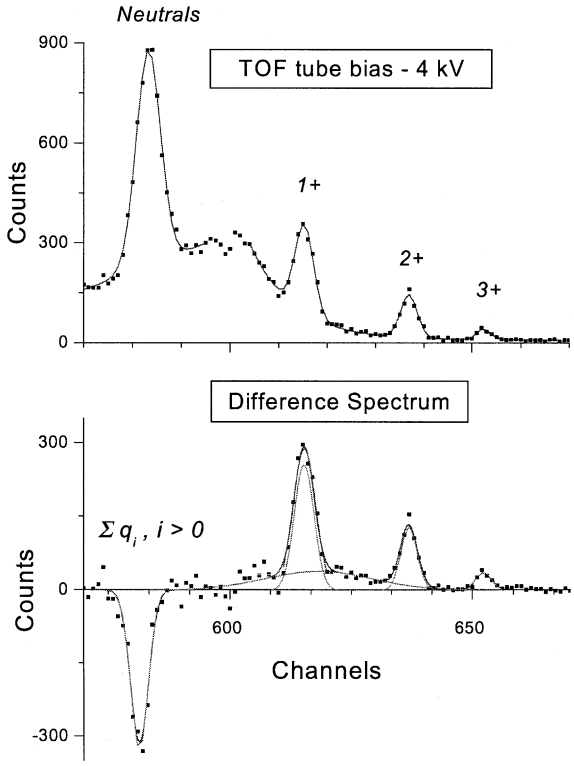

Fig. 1. Experimental TOF spectrum for Ar^{9+} normally incident on Au(1 1 0) at 20 keV, showing the scattered charge dispersion obtained by biasing the flight tube at −4.0 kV (thick lines), and the difference spectrum obtained by subtracting the corresponding grounded flight tube spectrum, used to eliminate much of the neutral multiple collision background, and to determine the detection efficiency of the MCP, as described in [10]. The curves shown are the results of non-linear multiple-Gaussian fits obtained using ORIGIN Pro 6.1, and illustrate the method of obtaining the peak areas for the various scattered charge states.

from the figure, the spectrum exhibits rather sharp peaks originating from *elastic* BCs between the incident projectile and individual target atoms. The peaks due to non-neutral scattered charge states sit on the falling slope of a broad structure associated with scattered neutrals that have undergone multiple collisions. The non-neutral BC peaks are stripped from this 'background' continuum by subtraction of an auxiliary spectrum obtained with the flight tube at zero potential, the result of which is the "difference" spectrum also shown in the figure. Both the shape and intensity of the multiple collision background, as well as the intensities of quasi-BC peaks, are strong functions of incidence angle and target azimuthal orientation, as has also been found in the case of singly charged incident ions [12]. The multiple collision background, while being a major structure in the scattered neutral spectra, is not a significant feature in the non-neutral scattered charge state spectra, indicating very low survival probabilities of non-neutral scattered projectiles in multiple collisions for the present case. Prior to determination of the absolute scattered charge fractions shown in a later section, the background-subtracted binary-collision-peak areas of the various scattered charge states are corrected for collection and detection efficiency effects as has been previously described [10].

3. Computer trajectory simulations

To understand incidence angle and target azimuthal orientation dependences of the scattered fluxes, projectile trajectory simulations using the MARLOWE (version 14c) code [7] were carried out. MARLOWE treats the interaction between the projectile and the surface in an *elastic* BC approximation (BCA). An exponential-sum screened Coulomb interaction potential was chosen with default parameters from [13], and a (2×1) reconstruction of the Au(1 1 0) surface was assumed [14,15]. The primary beam energy distribution was simulated in a series of MARLOWE tasks with different initial particle kinetic energies. Due to computing time constraints the angular acceptance was increased by a factor of 4 over the experimental acceptance angle of 2°. Of the 4×10^6 trajectories generated for each target orientation investigated, about (0.03–0.08)% were scattered into the detector acceptance cone. For the latter trajectories, the number of collisions, scattering angles, etc. were saved, permitting their subsequent reconstruction.

The simulations were used as the basis for analyzing the collision events contributing to the "BC" peaks seen experimentally. They reveal that the BC peak is in fact built up from two kinds of events – pure single SC and "quasi-binary" double DC collisions. By quasi-binary is meant that class of double (and triple) collisions, usually a combination of large angle ("hard") and one or more small angle ("soft") scattering events that do not lie in the same plane, resulting in final energies encompassed in the observed main BC energy loss peak. The quasi-binary DC events are particularly prominent for scattering along the [1 0 0] target azimuth direction, i.e. *across* the missing rows of the reconstructed Au(1 1 0) surface. These collisions are to be distinguished from the true double collisions noted by, e.g. Huang et al. [1], which are characterized by roughly 18% higher scattered energies. Higher multiplicity events (i.e. number of collisions >2) do not contribute to the BC peak, and form instead the pedestal upon which the peak sits. The relative contributions of true binary and quasi-binary double (and at higher energy, triple) collisions to the BC peak vary strongly with target azimuth, and underlie the measured azimuth variations of scattered charge fractions that will be shown in a later section.

An analysis of the target layers in which the events making up the BC peak occur for our geometry, shows that single collisions in only the top three target layers contribute. They are denoted SI, SII, and SIII, respectively. Target atoms not directly at the surface/vacuum interface have negligible contribution to the BC peak, presumably resulting from shadowing effects due to our near normal incidence conditions. The hard-soft-quasi-BCs originate exclusively from the second and third target layers and will be denoted DII and DIII, the Roman numeral designating the layer in which the hard collision occurs. Fig. 2 shows these five collision types as well as their individual target

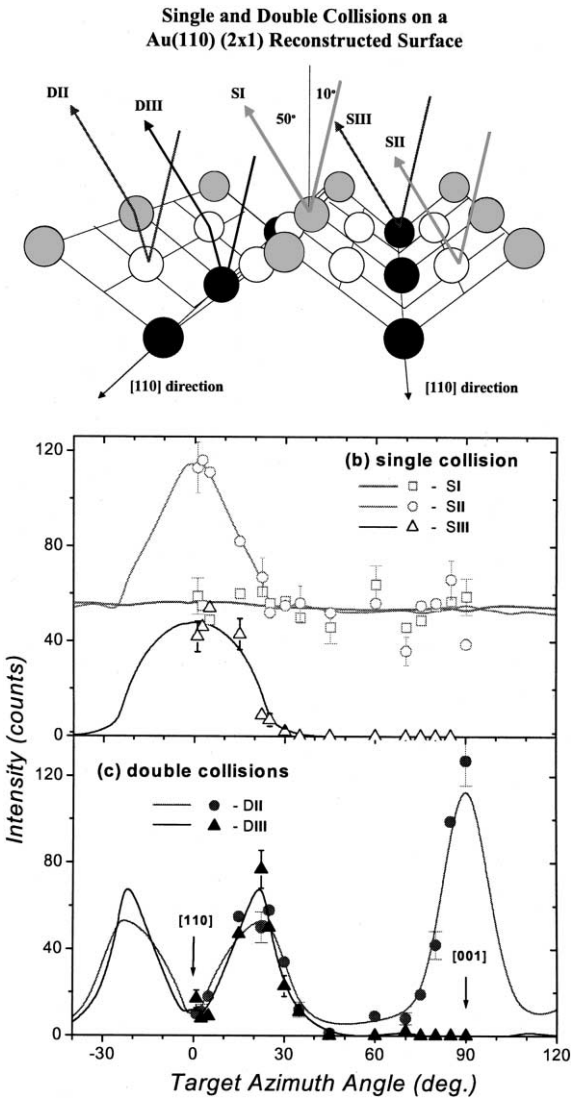

Fig. 2. Simulation results of the azimuth dependence of each of the quasi-BC types, shown at the top of the figure, occurring in the first three target layers; for 5 keV Ar projectiles incident on Au(1 1 0) at 10°.

azimuth dependences for 5 keV Ar projectiles incident at 10°, together with a schematic representation of the (2×1) reconstructed Au(1 1 0) surface. A striking feature of the simulation results is that each collision type is characterized by a distinct and unique dependence on target azimuth.

4. Experimental and simulation results at 20 keV

Fig. 3 shows the measured target azimuth dependence of the total (i.e. summed over all scattered charge states) scattered flux as well as that of the individual scattered charge states for 20 keV Ar^{9+} normally incident on Au(1 1 0). The figure also shows fits to the experimental azimuth dependences based on MARLOWE simulations as described below. The experimental results shown in Fig. 3 are qualitatively very similar to those shown in [3,4]. The neutral scattered charge fraction shows the greatest variation with target azimuth orientation, with primary and secondary maxima in the vicinity of the [1 1 0] and [1 0 0] directions, respectively, and a minimum in the azimuth range 40–70°, while the higher scattered charge fractions show significantly smaller modulation as function of target azimuth. As discussed

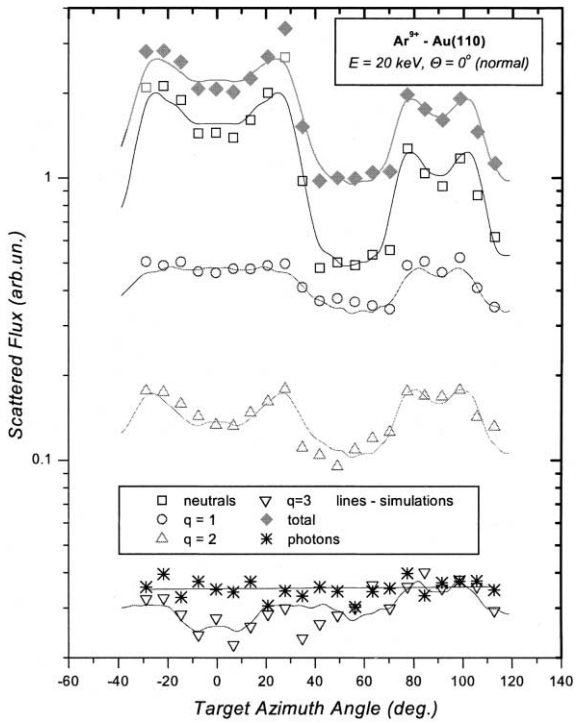

Fig. 3. Measured target azimuth dependence of scattered projectile charge fractions for 20 keV Ar^{9+} ions normally incident on Ar(1 1 0). The solid lines are fits to the different scattered charge states using MARLOWE simulation results as outlined in text.

previously [3,4] and below, these modulations result from the azimuthal variation of the contributions of SC and quasi-binary multiple collisions to the formation of a particular final scattered charge state.

In contrast to our results at 5 keV with 10° incidence angle, simulations at 20 keV and normal incidence using the MARLOWE default "collision" criterion (maximum impact parameter $b_{max} < 1.6$ Å) give the result that the projectile interactions with the top layer are comprised of both single and double collisions. This arises from the fact that, for normal incidence and 120° scattering along the [1 1 0] direction, the receding projectile passes by the next lattice site along the row (in-plane) with an impact parameter of about

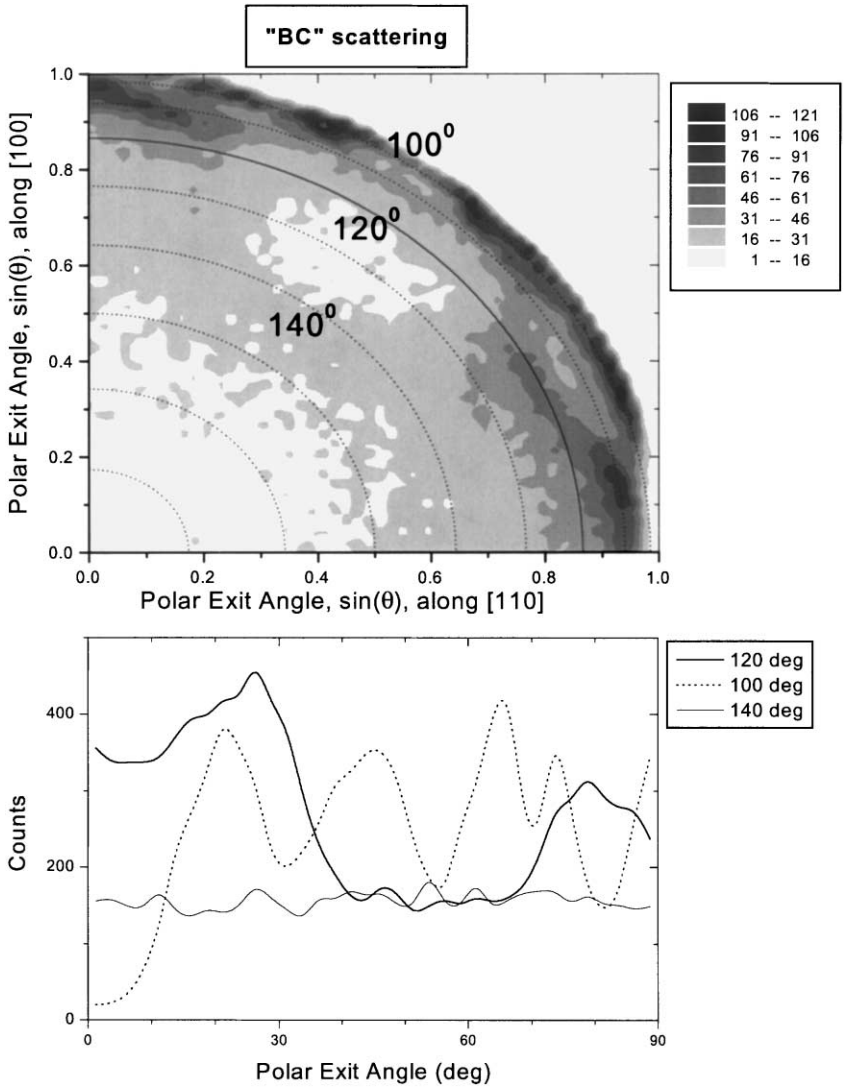

Fig. 4. (Top): simulated contour plot of the scattered flux distribution over polar and azimuthal exit angles for 20 keV Ar projectiles normally incident on Au(1 1 0). (Bottom): cuts of the total flux azimuth distribution shown in the top plot at three different polar exit angles.

Table 1
Scattered charge fractions and the mean charge for SI and SII collisions from 20 keV Ar^{9+} incident projectiles normally incident on Au(1 1 0), compared to earlier results at 5 keV. Note that the 20 keV values were obtained from fits in which the maximum impact parameter for a charge exchange collision was reduced from the MARLOWE default value of 1.6 to 1.22 Å

Outgoing charge state	20 keV Ar^{9+}		5 keV Ar^{9+}	
	SI	SII	SI	SII
0	0.24	0.80	0.37	1.00
+1	0.55	0.15	0.58	0.00
+2	0.17	0.04	0.042	0.00
+3	0.04	0.005	0.006	0.00
Mean charge	1.01	0.245	0.68	0.0

1.4 Å, i.e. less than b_{max}. This impact parameter is significantly greater than that expected for the quasi-binary (out-of-plane) DC events included in the 5 keV simulations when scaled to the higher collision energy considered here. More importantly, the azimuthal dependences of the collision types that are obtained using the MARLOWE default collision criterion are no longer as unique as was the case for 10° incidence at 5 keV. Specifically, the DI, DII, and DIII events all show pronounced maxima in the [1 1 0] direction, while both SI and SII now show azimuthally flat distributions away from the [1 0 0] direction. Since the quasi-binary DC impact parameters along the [1 0 0] direction at 5 keV were 0.133 and 1.14 Å, respectively (see footnote 19 of [3]), and since it is reasonable to assume that neutralization distances decrease with increasing projectile energies, we have performed an alternate sorting of the MARLOWE results, in which a maximum distance for charge transfer of 1.2 Å was assumed. This reduced cut-off distance had the effect of eliminating the (spurious) DI collision type, and of essentially recovering, in general, the azimuth dependences of the various collision types obtained in the earlier MARLOWE simulation for 10° incidence at 5 keV. The simulation agreement with the total observed scattered charge flux (i.e. summed over all charge states) was, of course, not affected by the above change in the default charge exchange distance, since the latter results only in a redistribution of collision types.

The remaining difference between the 5 and 20 keV results, i.e. the double, instead of single, maximum in the vicinity of the [1 0 0] direction, is also ascribed to the difference in incidence angles at the two energies. The simulation reveals that the double maximum arises mainly from quasi-binary double and triple collisions originating in the second and third layers that become possible over a small range of azimuths on either side of the [1 0 0] direction.

Using the excellent agreement of the total observed and simulated scattered fluxes as justification, as was done previously [3], we assessed the relative contributions of the different collision classes by fitting the measured fluxes of the different scattered charge states by weighted linear combinations of the five identified collision types, in a manner similar to that outlined in [3,4]. The obtained fits are shown as the solid lines in Fig. 4. The scattered charge fractions resulting from the different contributing collision types could thus be deduced, as has already been discussed elsewhere [3]. The scattered charge fractions for the SI and SII collision type deduced in this manner are summarized in Table 1, together with a comparison of the corresponding results for Ar^{9+} incident at 5 keV already presented in Ref. [4]. A more complete tabulation that includes the other three collision types is deferred to a later publication.

When comparing the present measured and fitted charge fraction azimuth dependence for the 1+ scattered charge state with our previous results for 5 keV (see [4]), it is noted that the sinusoidal modulation versus azimuth seen at the lower energy is no longer evident. As discussed in greater detail in [4], this sinusoidal behavior implied a charge exchange process arising from a collective interaction with target rows along the [1 1 0] direction at distances that exceeded the MARLOWE collision criterion of 1.6 Å, and which therefore lay outside the scope of the MARLOWE simulation. Its absence at 20 keV supports the above-stated assumption that neutralization distances decrease with increasing energy, and provides some justification of decreasing the charge exchange critical distance below the MARLOWE default value. An important conclusion from this discussion is that charge exchange (i.e. neutralization) critical

distances in hard collisions must be determined independently of MARLOWE, and that the generally good agreement found at 5 keV, where the neutralization critical distance was in effect set equal to the MARLOWE b_{max}, may have been somewhat coincidental.

5. Simulation sensitivity studies

In this section we present some auxiliary simulation studies that explore the effects of changing the total scattering angle, details of the scattering potential, and type of surface reconstruction assumed. The first study was aimed at optimization of the scattering geometry specifically for a Au(1 1 0) surface. The second was carried out in part to assess the extent to which details of the azimuthal dependences were influenced by the scattered projectile charge states themselves. The third was undertaken to see what information about the surface topography itself that the observed azimuth dependences of the scattered projectiles provided.

5.1. Total scattering angle

When looking along the [1 1 0] direction, the reconstructed Au(1 1 0) surface has a characteristic projected opening angle of about 109°. Ions with 10° incidence angle undergoing 120° backscattering thus seem well suited for probing the effects of the local corrugation of the missing row surface structure on projectile. In an attempt to find support for this intuitive picture, backscattering simulations were made for normal incidence in which the constraint of scattering into a particular detector solid angle was lifted, and all valid quasi-binary backscattering events were instead recorded by exiting polar and azimuthal angle. The result of this simulation, carried out at for 20 keV Ar projectiles, is shown in the top of Fig. 4, where the number of events into a given direction is indicated by the greyscale to the right of the figure. The lower part of the figure shows three cuts of this data for three different total scattering angles, including the 120° at which the measurements were carried out. Interestingly enough, at the larger scattering angle of 140° the azimuthal variation of the total scattered flux has largely disappeared, while at the smaller scattering angle of 100° the azimuthal dependence shows much more complex oscillatory behavior with multiple periodicities. Both types of dependences would make application of the fit procedure outlined above more problematic that was the case for 120°. Since the 120° scattering angle in the present set-up was fixed in the design stage and is not easily changeable, Au(1 1 0) was, in hindsight, an excellent choice of target to investigate by this means.

5.2. Scattering potential

The simulations used in our work to date used the ZBL [13] screened Coulomb potential appropriate for collisions between Au and Ar (i.e. Z_{Target} and $Z_{Projectile}$ equal to 79 and 18, respectively). In view of the progressively higher non-neutral scattered charge fractions observed as the projectile charge and/or energy are increased, we investigated possible effects on the simulated azimuth dependences of deviations from a pure screened Coulomb scattering potential. To this end we explored two changes in the scattering potential: simulating the effect of a surviving inner shell vacancy by increasing $Z_{Projectile}$ from 18 to 19, and in a separate run adding to the ZBL potential a pure $1/R$ term (without screening), as a rather more extreme modification. While the different scattering potentials result in some minor changes to the over-all azimuthal dependence of the scattered flux, they are smaller than the combined uncertainties of the experimentally determined total flux distribution, estimated at $\pm 15\%$, and of the simulations, which comprised about 200 events in the peak of the distribution. It is not clear whether the only minor change seen with the addition of the $1/R$ term is due to a true insensitivity of the overall scattering to this term, or to a limitation of MARLOWE, which treats the ion surface interaction as a series of BCs connected by straight line segments.

5.3. Surface reconstruction

An additional aspect we explored is the extent to which the (2×1) surface reconstruction of

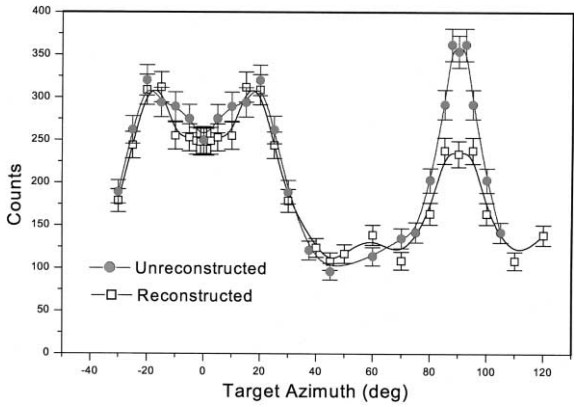

Fig. 5. Simulated azimuth dependences of the total scattered projectile flux for 5 keV Ar projectiles normally incident on a reconstructed (i.e. having missing rows) and non-reconstructed (i.e. no missing rows) Au(1 1 0) surface.

Au(1 1 0) manifested itself in the experimental and simulation results. To this end, we compared the simulated azimuthal dependences of scattered Ar projectiles incident normally at 5 keV on both reconstructed (i.e. having "missing rows") and unreconstructed (no missing rows) Au(1 1 0) surfaces. As can be seen from Fig. 5, there is a significant enhancement of quasi-binary scattering along the [1 0 0] direction, i.e. across the missing rows, which corresponds quantitatively with the doubling of the number of scattering lattice sites in the top layer when the missing rows are filled in. The excellent agreement of the reconstructed surface simulation results with our experimental data, carried out at samples temperatures in the range 300–450 K, confirms the expected (2×1) reconstruction of Au(1 1 0) at temperatures below the 650 K phase transition [16].

Acknowledgements

This research was sponsored in part by the Office of Fusion Energy Sciences, and by the Office of Basic Energy Sciences of the US Department of Energy under contract no. DE-AC05-00OR22725 with UT-Batelle, LLC. V.A.M was appointed through the ORNL Postdoctoral Research Associates Program administered jointly by Oak Ridge Associated Universities and ORNL.

References

[1] W. Huang et al., Phys. Rev. A 56 (1997) 3777.
[2] W. Huang et al., Phys. Rev. A 58 (1998) 2962.
[3] V.A. Morozov, F.W. Meyer, Phys. Rev. Lett. 86 (2001)736.
[4] V.A. Morozov, F.W. Meyer, Phys. Scripta T 92 (2001) 31.
[5] F.W. Meyer et al., Phys. Scripta T 92 (2001) 182;
F.W. Meyer, V.A. Morozov, J. Mrogenda, C.R. Vane, S. Datz, Nucl. Instr. and Math. B 193 (2002) 508.
[6] Q. Yan et al., Phys. Rev. A 54 (1996) 641;
F.W. Meyer et al., Nucl. Instrum. Meth. B 125 (1997) 138.
[7] M.T. Robinson, Radiat. Eff. Defect Solid 130 (1994) 3;
M.T. Robinson, Phys. Rev. B 40 (1989) 10717.
[8] A. Arnau et al., Surf. Sci. Rep. 27 (1997) 113, and references cited therein;
H.P. Winter, F. Aumayr, J. Phys. B 32 (1999) 39, and references cited therein.
[9] F.W. Meyer, V.A. Morozov, Nucl. Instrum. Meth. B 157 (1999) 297.
[10] V.A. Morozov, F.W. Meyer, Rev. Sci. Instrum. 70 (1999) 4515.
[11] F.W. Meyer, V.A. Morozov, Phys. Scripta T 80 (1999) 226.
[12] E. Taglauer, W. Englert, W. Heiland, Phys. Rev. Lett. 45 (1980) 740;
T.M. Buck et al., Surf. Sci. 90 (1970) 635.
[13] J.F. Ziegler, J.P. Biersack, U. Littmark, The Stopping and Range of Ions in Solids, Vol. 1, Pergamon Press, New York, 1985, p. 48.
[14] W. Moritz, D. Wolf, Surf. Sci. 88 (1979) L29.
[15] R. Koch et al., Appl. Phys. A 55 (1992) 417.
[16] J.C. Campuzano et al., Phys. Rev. Lett. 54 (1985) 2684.